Published in final edited form as:
Nanomedicine (Lond). 2011 September ; 6(7): 1175–1188. doi:10.2217/nnm.11.41.

Macrophage scavenger receptor A mediates the uptake of gold colloids by macrophages *in vitro*

Angela França[1], **Parag Aggarwal**[2], **Eugene V Barsov**[2], **Serguei V Kozlov**[2], **Marina A Dobrovolskaia**[2], and **África González-Fernández**[†,1]

[1]Immunology, Biomedical Research Center (CINBIO), Universidad de Vigo, Campus Lagoas Marcosende, 36310 Vigo, Pontevedra. Spain

[2]SAIC-Frederick Inc., NCI-Frederick, Frederick, MD 21702, USA

Abstract

Aims—While numerous studies have reported on nanoparticle uptake by phagocytic cells, the mechanisms of this uptake are poorly understood. A metastudy of research focusing on biological particulate matter has postulated that nanoparticles cannot be phagocytosed and therefore must enter cells via pinocytosis. The purpose of this study was to identify the route(s) of uptake of gold nanoparticles *in vitro* and to determine if these route(s) depend on particle size.

Materials & Methods—The parent RAW264.7 cell line and its derivatives, transduced with a virus carrying siRNA to macrophage scavenger receptor A, were used as model phagocytes. Citrate-stabilized gold colloids were used as model nanoparticles. We used chemical inhibitors known to interfere with specific routes of particulate uptake. We developed multifocal light microscopy methods including multifocal stack analysis with NIH ImageJ software to analyze cell uptake.

Results—Irrespective of size, gold nanoparticles are internalized by macrophages via multiple routes, including both phagocytosis and pinocytosis. If either route was blocked, the particles entered cells via the other route.

Conclusion—Gold nanoparticles with hydrodynamic sizes below 100 nm can be phagocytosed. Phagocytosis of anionic gold colloids by RAW264.7 cells is mediated by macrophage scavenger receptor A.

Keywords

cellular uptake; gold nanoparticle; phagocytosis; pinocytosis; scavenger receptor

Nanoparticles represent a wide class of materials with different chemical compositions, architectures and physical properties. When nanoparticles enter the body, either intentionally (e.g., are administered during medical applications) or accidently (e.g., through environ mental exposure), they encounter a complex environment of macromolecules, including

[†]Author for correspondence: africa@uvigo.es.

Financial & competing interests disclosure The authors have no other relevant affiliations or financial involvement with any organization or entity with a financial interest in or financial conflict with the subject matter or materials discussed in the manuscript apart from those disclosed.

Ethical conduct of research The authors state that they have obtained appropriate institutional review board approval or have followed the principles outlined in the Declaration of Helsinki for all human or animal experimental investigations. In addition, for investigations involving human subjects, informed consent has been obtained from the participants involved.

proteins, lipids and cells. One of the first biological objects nanoparticles encounter upon entering the bloodstream are plasma proteins (opsonins) and immune cells. Nanoparticles are often removed from circulation by resident phagocytic cells of the liver and spleen. One of the great potential benefits of nanotechnology is that it allows researchers to 'engineer around' undesirable biological events (such as excessive endocytosis by immune cells) by altering nanoparticle physicochemical properties; nanoparticles can be coated with polymers (e.g., polyethylene glycol) to reduce uptake or, if more internalization is desired, engineered to target phagocytic cells to accelerate uptake and antigen presentation.

Multiple studies have documented internalization of nanoparticles by macrophages; however, no detailed delineation of the uptake pathway has been reported [1–3]. This is probably due to limitations of visualization technology for particles inside cells. Highly sensitive techniques, such as transmission electron microscopy (TEM) and scanning electron microscopy are useful to detect electron dense materials (e.g., metallic nanoparticles, gold nanoshells, iron oxides and TiO_2 particles). For example, TEM and atomic force microscopy have been used to document uptake of gold colloids by macrophages and cancer cells [1,2,4]. But such techniques cannot reliably image polymers, dendrimers, nanoliposomes or other 'soft' materials on the size scale of cellular organelles, without recourse to cryogenic techniques or staining. In addition, TEM images are 2D slices, which may not accurately represent entire 3D cells. In addition, heavy metals used in TEM sample preparation often leave high density marks, which may be mistaken for nanoparticles, requiring elemental analysis through techniques such as TEM-energy dispersive x-ray spectroscopy for definitive measures, thus making this method costly and low throughput. Since reliable direct visualization of soft particles is difficult, most studies use indirect assays for phagocytosis (e.g., luminol-based detection or flow cytometry). Luminol detection offers high sensitivity, but is limited by the extent to which a particle quenches the luminol signal while inside the cell. Flow cytometry assays for phagocytosis cannot distinguish between particles attached to the cell membrane and internalized particles. Nevertheless, limited studies have reported that approximately 90-nm mannose-coated nanoemulsions, 130-nm mannose-chitosan nanoparticles and 200-nm gluco–mannan particles are internalized by macrophages via the mannose receptor-mediated phagocytic pathway [5–7], whereas 20-, 50- and 100-nm lipid nanocapsules exploit a complement receptor-mediated internalization pathway[8]. Other data also suggest that fullerene derivatives may be phagocytosed via the Fcγ receptor (FcγR) route [9,10]. Phagocytosis of microbial pathogens via these pathways frequently results in inflammatory cytokine production, and similar inflammatory response has been also documented with other particles. Of interest are studies with 10–20-nm superparamagnetic nanoparticles, which demonstrated uptake via Mac-1 receptor [11] and, 20-, 50- and 200-nm anionic polystyrene particles, which demonstrated uptake via scavenger receptor (SR) [12,13]. SR-mediated uptake is a 'classical' pathway utilized by macrophages to eliminate apoptotic cells and is not accompanied by proinflammatory cytokine secretion [14]. It has been reported that ferumoxtran-10 (dextran-coated superparamagnetic iron oxides) does not induce inflammatory cytokines [15], likewise no cytokine secretion has been reported for polystyrene particles [12,13]. Another challenge in studying nanoparticle uptake is the absence of a standardized means for quantification. For example, in traditional immunology, phagocytosis is quantified by the number of bacterial cells, yeast or poly styrene beads inside an individual phagocytic cell and, reported as the average number of ingested bacteria (yeast or beads) per cell. This measurement is called the 'phagocytic index'. The number of cells demonstrating uptake is used to calculate the 'percentage of active phagocytes'. The general rule is to count at least 100 cells to determine the values of the phagocytic index and the percentage of active phagocytes. Such quantifiers cannot be used to study nanoparticle uptake, since all the available techniques are not sensitive enough to provide individual particle counts inside cells. To overcome this obstacle, we have developed a method based on multi focal imaging of at least 100 cells per sample, followed

by multifocal image analysis using NIH ImageJ software, which measures high-density areas inside cells. We then express phagocytic index as the mean area per cell.

Some earlier studies have attempted to draw general rules for nanoparticle uptake, suggesting, for example, that particles less than 100 nm in diameter enter cells via pinocytosis, while larger particles (above 100 nm) are phagocytosed [16]. This conclusion was based on a metastudy of basic research focusing on the uptake of biological particulate matters (e.g., viruses, bacteria and model polystyrene beads) and therefore should be tested on a variety of nanoparticles before it is concluded to apply to all engineered nanoparticles. In the present study, we used commercially available citrate-stabilized colloidal gold nanoparticles of two different sizes – one below 100 nm and the other above 100 nm, as a test case to see if this rule extends to nanoparticles.

We chose gold nanoparticles because gold has a long history of biomedical use. Gold salts have been used to reduce inflammation and gold colloids are used as drug delivery vehicles, with some applications in clinical trials [17,18,101,102]. Gold colloids are often modified with polyethylene glycol in order to avoid unspecific uptake by the reticuloendothelial system [18]. It is worth noting, if the polyethylene glycol coatings are not stable during storage or dissociate when the colloids enter the bloodstream, immune cells will clear them, leading to potential long-term toxicity, as the colloids accumulate in the liver, spleen and other lymphoid organs. Thus understanding the route of uptake of colloidal gold particles is of interest from both basic and translational research perspectives.

Several previous studies have suggested that unmodified water-soluble gold nanoparticles can enter cells via pinocytosis [1], and that modification of particle surfaces with various ligands can direct the uptake of gold nanoparticles to specific receptors [1–4]. However, none of these studies have investigated entry routes of colloidal gold nanoparticles into macrophages.

The purpose of the current study, was to understand whether particle size influences the route through which gold particles enter into macrophages and to test general rules derived from research on other particulates. We show that irrespective of size, the citrate-stabilized gold colloids enter the macrophages via multiple routes, including both pinocytosis and phagocytosis, and that uptake via the SR is a primary pathway for phagocytosis of gold colloids.

Material & methods

Reagents

Colloidal gold nanoparticles with sizes of 30 and 150 nm were purchased from TedPella Inc (CA, USA). Particle size was characterized by dynamic light scattering and TEM. Characterization also included measuring zeta potential and determining endotoxin levels. For the endotoxin levels measurement by kinetic turbidity limulus amebocyte lysate (LAL), PyrosKinetix instrument, endotoxin standard, LAL-grade water and lysate were used and all were purchased from Associates of Cape Code Inc. (ACC, MA, USA). The LAL test was performed according to the manufacturer's instructions (ACC). For the inhibition experiments, the following reagents were used: cytochalasin D (0.2, 1 and 5 μM); 5-(*N*,*N*-dimethyl) amiloride hydrochloride (2 and 10 μM); chlorpromazine hydrochloride (2 and 5 μM) and filipin III (0.5 mg/ml), all were supplied by Sigma-Aldrich (MO, USA). The eight-well LabTech chamber slide used for the uptake experiments were supplied by Fisher Scientific (PA, USA). Goat antimouse SR-A1/MSR1 neutralizing antibodies (2 and 5 μg/ml) and isotype control Goat IgG antibodies (5 μg /ml) were purchased from R&D systems (MN, USA), antibodies directed against murine β-actin were supplied by ABcam (MA,

USA) and horseradish peroxidase-conjugated secondary antibodies were supplied from Jackson ImmunoResearch Labs (PA, USA). The adherent RAW264.7 murine macrophage cell line was obtained from American Type Culture Collection® (MD, USA). All cell culture reagents, fetal bovine serum (FBS), phosphate buffered saline (PBS), RPMI and Dulbecco's Modified Eagle medium (DMEM) were supplied by Hyclone (MA, USA). FBS was heat inactivated for 30 min at 56°C before use for cell culture. The 10% neutral buffered formalin solution, phytohemagglutinin-M (PHA-M) and gamma-irradiated cell culture grade *Escherichia coli* O55B5 l lipopolysaccharide were all purchased from Sigma Aldrich. The human AB^+ serum used was supplied by BioChemed (VA, USA). The Packaging GP2–293 cells were supplied by Clontech (CA, USA). The selection of sequences for the most optimal RNAi-mediated inhibition was guided by BLOCK-iT™ RNAi Designer tool purchased from Invitrogen (CA, USA) and the final oligonucleotides were made compatible with the XhoI and EcoRI cloning sites of the shRNAmir lentiviral vector MSCV/LTRmiR30-PIG (LMP) from Open BioSystems (AL, USA). For the gene ration of retroviral vectors stocks and for the retroviral transduction of RAW264.7 cells were used, respectively, the TransIT-293 reagent supplied by Mirus Bio, (WI, USA) and ViroMag R/L Viral Gene Delivery reagent from Boca Scientific (FL, USA). For the cytokine secretion test, the Th1/Th2 kit from Mesoscale Discovery (MSD) Inc. (MD, USA) was used. Plasma samples were analyzed for the presence of complement split products using C4d, iC3b and Bb EIA kits from Quidel Corporation (CA, USA). To analyze expression of SR-A, 4× NuPAGE buffer and 10× reducing agent supplied by Invitrogen were used. Trisglycine gels were purchased from Invitrogen. Ficoll Paque Plus reagent was supplied by Amersham Biosciences (Upsala, Sweden).

Research donor blood

Healthy volunteer blood specimens were drawn under the NCI-Frederick Protocol OH99-C-N046 approved by the institutional internal review board. Blood was collected in BD vacutainer® tubes containing sodium citrate as an anticoagulant (for complement activation assay) or lithium heparin (for cytokine secretion assay). For opsonization of nanoparticles, we used human AB^+ serum (BioCheMed, VA, USA).

Dynamic light scattering

A Malvern Zetasizer Nano ZS instrument (MA, USA) with back scattering detector (173, 633 nm laser wavelength) was used for measuring the hydrodynamic size (diameter) in batch mode at 25°C in a low volume quartz cuvette (pathlength 10 mm). Citrate-stabilized gold nanoparticles samples were diluted tenfold in 10 mM NaCl and filtered through a 0.45-μm filter. A minimum of 12 measurements per sample were made. Hydrodynamic size is reported as the intensity-weighted average (Int-Peak) diameter.

Zeta potential

A Malvern Zetasizer Nano ZS instrument was used to measure zeta potential at 25°C. Citrate-stabilized gold nanoparticles samples were diluted tenfold in 10 mM NaCl. An applied voltage of 100 V was used. Samples were loaded into prerinsed folded capillary cells and a minimum of three measurements were made per sample.

Cell culture

The adherent RAW264.7 murine macrophages cell line was used throughout this study. The cells were cultured in RPMI supplemented with 10% (v/v) heated-inactivated FBS, 2 mM glutamine and 100 units per ml of penicillin/ streptomycin solution at 37°C in 5% CO_2. Cells were split every other day to maintain 70–80% confluent cultures. Cells were used between passages 3 and 20; after passage 20, cultures were discarded and new cultures were

started from frozen stocks. Cells were screened for mycoplasma contamination (no contamination was detected).

Packaging GP2–293 cells (Clontech) were maintained in DMEM supplemented with 10% FBS and penicillin/streptomycin (100 units/ml).

Generation of SR-negative cell line

Based on the cDNA sequences of *Mmsr1* and *Mmsr2* genes, eight pairwise complimentary oligonucleotides have been designed (Box 1) (only sense oligonucleotide are shown), to produce four independent siRNA constructs for each gene. The selection of sequences for optimal RNAi-mediated inhibition was guided by BLOCK-iT RNAi Designer tool (Invitrogen) and the final oligonucleotides were made compatible with XhoI and EcoRI cloning sites of shRNAmir lentiviral vector MSCVLTRmiR30-PIG (LMP; Open BioSystems).

Generation of retroviral vector stocks

Packaging GP2–293 cells were cotransfected with each of the shRNA plasmids and vesicular stomatitis virus G protein (VSV-G) expression construct by using TransIT-293 reagent (Mirus Bio, WI, USA) according to the manufacturer's recommendations. Briefly, the mixture of shRNA construct (18 μg) and VSV-G vector with TransIT-293 (2 μg) was added to subconfluent GP2–293 culture in a 150 cm^2 flask, the cells were incubated for 24 h and the culture medium was replaced with the fresh medium. The virus-containing supernatant was harvested 48 h post-transfection and was clarified by centrifugation at 3000 rpm for 10 min. To concentrate the vector particles, clarified virus-containing supernatant was spun down at 21,000 × g for 2 h at +4°C, the pellet was resuspended in a small volume of the TNE buffer (50 mM Tris, pH 7.8, 130 mM NaCl, 1 mM EDTA) and was either used immediately to infect target cells or, was frozen at −70°C for long-term storage.

Retroviral transduction of RAW264.7 cells

Parent RAW264.7 cells were plated in the wells of a six-well plate in RPMI medium as described earlier at 10^5 cells per well and were grown overnight. The cells were transduced with corresponding retroviral vector by using ViroMag R/L Viral Gene Delivery reagent (Boca Scientific) according to the manufacturer's recommendations. Briefly, magnetofection reagent (8 μl) was added to concentrated retroviral vector stock (50 μl) and incubated for 30 min at room temperature. The mixture was added to target cells and the plate was placed behind a magnetofection magnet (Boca Scientific) and incubated for 2 h at 37°C. The plate was taken off the magnet and the cells were cultured for 48 h prior to selection with puromycin. Single cell colonies that passed the selection with puromycin were collected and subcultured in the presence of puromycin in a 96-well plate. Each clone was allowed to expand and was analyzed for the presence of scavenger receptor A1 (MSR-1) by western blot as described later. A total of 34 clones were harvested and analyzed. Two of these clones designated 4/2 C6 (originated from oligo construct #4) and 1/2 (originated from oligo construct #1) were used for further studies as they demonstrated no expression of MSR1, maintained adherent properties of the parent cells and showed no changes in uptake of Zymosan A.

Cytokine secretion, complement activation, protein electrophoresis & western blot

For the cytokine secretion test, human peripheral blood mononuclear cells were isolated from the whole blood of three healthy volunteers by Ficoll gradient centrifugation. Ficoll Paque Plus reagent was from Amersham Biosciences (Upsala, Sweden). Cells were incubated for 24 h in the presence of negative control (PBS), positive control:

lipopolysaccharide (LPS) and phytohemagglutinin from *Phaseolus vulgaris* (PHA-M), or nanoparticles. Cell culture supernatants were collected, cleared by centrifugation for 5 min at 18,000 × g and stored at −20°C before analysis. The analysis was performed using Th1/Th2 kit from MSD Inc. using a MSD plate reader, and following the manufacturer's instructions.

For complement activation, fresh (1–2 h postcollection) human plasma anticoagulated with sodium citrate and collected from at least three healthy donor volunteers was incubated for 30 min at 37°C with positive control (cobra venom factor), negative control (PBS) or nanoparticles in the presence of veronal buffer. Plasma samples were analyzed for the presence of complement split-products using C4d, iC3b and Bb EIA kits from Quidel Corporation (CA, USA). All experiments were performed according to manufacturer's instructions.

To analyze expression of SR-A, cell lysates were prepared on ice using lysis buffer (20 nM Tris HCl, pH 7.4, 5mM EDTA, pH 8.0, 1% w/v Triton X-100 and protease inhibitor cocktail). Lysates were mixed with 4× NuPAGE buffer (Invitrogen) and 10× reducing agent (Invitrogen) and incubated for 5 min at 85°C. Proteins were then separated using 10% trisglycine gels (Invitrogen) and transferred onto polyvinylidene fluoride membrane. Membranes were blotted with antibodies specific to murine SR-A1(MSR-1) and β-actin to control protein loading.

Uptake experiments

RAW264.7 cells were plated (1.5×10^5 cells/ml) in an eight-well plate (Nunc Lab-Tek Chambered Cover Glasses, Fisher Scientific, USA) 1 day prior to the experiment. The culture media was removed and the cells were treated with inhibitors for 1 h. The uptake studies were started by adding the nanoparticles (~50 μg/ml) suspended in culture media to the cells. The process was stopped by three washes with PBS, then 10% neutral buffered formalin solution was added for 15 min. To obtain a proper depth-of-image of the nanoparticles within the cells, images were taken at different focal points and then combined. The images were taken at 1000× magnification using a Nikon microscope with a 10× eyepiece and a Plan Fluor 100×/1.30 Oil Ph3 DLL Objective. Stacking of the images into one multifocal stack and densitometry were performed using NIH ImageJ software. The entire stack was prefocused into one image through a stack focuser (a plugin to NIH ImageJ) to obtain the final image. The relative image intensity of each cell was calculated and compared with other cells and control cells. After correcting for the background, these values were compared to obtain the relative intensity, which correlates with the relative amount of nanoparticles in the cells. For each treatment and control sample, a total of 100 cells were analyzed. Each cell was imaged multiple times, scanning from the bottom to the top and the stacked multifocal image representing the entire cell was used for analysis. The analysis of each data set was performed by two scientists independently. Phagocytosis was rated as phagocytic index, which represented an average density value calculated by analyzing 100 cells. Percentage uptake was calculated by counting the number of cells (out of 100) with increased density over background and comparing the phagocytic index values of these cells to control samples. For this purpose, the phagocytic index in control samples were assigned 100% uptake and the test samples were compared with this control. For protocol details and validation experiments please refer to Supplementary Data and appendix A (see online www.futuremedicine.com/doi/suppl/10.2217/nnm.11.41).

Statistical analysis

The mean values were compared by one way ANOVA analysis using Microsoft Excel 2007 software. Statistical significance was accepted for $p < 0.05$. The images were analysed by NIH ImageJ and the intensity results are expressed as mean area, in μm^2.

Results

Particle characterization

Dynamic light scattering is a common method for determining the hydrodynamic size (diameter) of a nanoparticle in solution. Nanoparticle hydrodynamic size can be altered by the presence of opsonizing proteins and, is often more relevant to interaction with biological systems than the core size [19,20]. Therefore, we measured hydrodynamic diameter both before and after incubation with serum. We also evaluated the particles' core size by TEM (data not shown) and measured particle zeta potential. Since endotoxin contamination may confound results of *in vitro* studies such as cytokine secretion tests [21], we also determined the amount of endotoxin in commercial stocks of 30- and 150-nm gold colloids.

The results of particle characterization are summarized in Table 1. The hydrodynamic sizes of 30-nm gold colloids were determined to be 34.4 ± 0.2 nm before opsonization and 94.8 ± 0.2 nm after incubation with serum; those of 150-nm particles were 149.8 ± 0.7 nm and 263.6 ± 4.7 nm before and after opsonization, respectively. The zeta potential of the 30-nm gold colloids was −38.2 ± 1.2 mV before and −16.4 ± 0.6 mV after incubation with serum; those of 150 nm particles changed from −46.3 ± 0.9 mV before to −20.4 ± 1.9 mV after the opsonization. The amount of gold was comparable in both formulations: 48.0 ± 3.9 μg/ml and 42.5 ±3.7 μg/ml in 30- and 150-nm colloids, respectively. Endotoxin was below the limit of detection.

Selection of inhibitors & dose metrics

Mammalian cells have two main endocytic portals for internalization of the macromolecules and particles: phagocytosis and pinocytosis [22]. The former is further subdivided into complement receptor-mediated, FcγR-mediated and SR-mediated phagocytosis. Pinocytosis is also subdivided into categories, including macropinocytosis, clathrin-mediated, caveolin-mediated and clathrin/caveolin-independent endocytosis [22,23]. Each pathway involves a unique set of receptors and is employed only for particular types of particulate material. To distinguish between the pathways, we utilized a set of commercially available inhibitors identified as having selective effects on specific uptake pathways. The inhibitors and their mechanisms of action are summarized in Table 2.

We found that dosing equal concentrations (equal numbers of gold particles per volume) approached our sensitivity limits for detection of the 30-nm colloids after administration of the uptake inhibitors (Supplementary Figure 1). To ensure a fair comparison of the uptake of 30- and 150-nm colloids, we therefore, dosed cells with nanoparticles at equivalent concentrations of total gold, so that both before and after administration of the uptake inhibitors, the 30- and 150-nm colloids were similarly detectable.

Inhibition of actin polymerization results in decrease in the uptake of both 30- & 150-nm gold colloids

One of the common features between phagocytosis and macropinocytosis is that both pathways represent active transport and require actin polymerization [22,23]. Therefore, we first tested cytochalasin D, an inhibitor of actin polymerization, for its ability to affect uptake of gold colloids by macrophages. Pretreatment of macrophages with cytochalasin D resulted in decreased uptake of both 30- and 150-nm gold colloids (Figure 1a). We observed

a similar decrease in uptake for nanoparticles of both sizes with a lower dose of the inhibitor. Increasing the concentration of the cytochalasin D exhibited a complex effect on uptake: the internalization of the large-size colloids (150 nm) was affected to a greater degree (>50%) than that of smaller (30 nm) colloids.

To further distinguish between these two routes of uptake, we used 5-(*N*,*N*-dimethyl) amiloride hydrochloride, the compound that inhibits the membrane Na^+/H^+ ATPase and is reported to inhibit macropinocytosis [24]. Treatment with 5-(*N*,*N*-dimethyl)amiloride hydrochloride did not result in a significant decrease in the uptake of either 30- or 150-nm gold colloids (Figure 1B).

SR is involved in the phagocytosis of 30-nm gold colloids

Two of the three aforementioned phagocytic routes, complement receptor and FcγR-mediated phagocytosis, result in triggering proinflammatory signaling, whereas SR-mediated uptake does not cause the induction of proinflammatory cytokines [14]. Neither 30- nor 150-nm gold colloids resulted in induction of inflammatory cytokines *in vitro* (Table 3). Likewise, no significant complement activation was observed with both tested colloids (Figure 2). Since no cytokine induction and no significant complement activation was observed, we focused on the SR-mediated pathway.

To evaluate the contribution of SR in the uptake of gold colloids, we employed two methods:

- Blocking SR by neutralizing goat antimouse SR-A1/MSR1 antibodies
- Using two clones of RAW264.7 cells (for the purpose of this study designated as RAW264.7-SR-negative) in which expression of SR is inhibited by specific siRNA (Figure 3E)

A decrease in the uptake of 30- and 150-nm gold colloids was observed in both parental RAW264.7 cells pretreated with neutralizing antibody (Figure 3A) and in RAW264.7-SR-negative cells (Figure 3B). The inhibition was more prominent with the smaller (30-nm) nanoparticles than the larger (150-nm) nanoparticles (Figure 3A). Isotype control results were more variable in the 150-nm experiment and resulted in some inhibition of gold uptake. This issue is addressed in detail in the discussion. Zymosan A uptake is largely dependent on complement receptor, therefore, we used zymosan A as a control. Uptake of the zymosan A was not affected in RAW264.7-SR-negative cells (Supplementary Table 1 & Supplementary Figure 2).

Clathrin-mediated pinocytosis is involved in the uptake of 30- but not 150-nm gold colloids

In order to further investigate routes of nanoparticle uptake by macrophages, we evaluated the clathrin-mediated pathway. Pretreatment of cells with chlorpromazine hydrochloride (a known inhibitor of the clathrin-mediated pathway) resulted in significant (close to 50%) inhibition of the uptake of the small (30 nm) nanoparticles, but had nearly negligible affects on uptake of the large (150 nm) gold colloids (Figure 3C). Because significant (~50%) decreases in the uptake were observed in the absence of SR (Figure 3a & 3B), and in the presence of clathrin-mediated endocytosis inhibitor (Figure 3C), we hypothesized that the uptake of 30-nm colloids could be almost completely blocked by coinhibition of both routes if these are the only two paths involved in uptake. To test this hypothesis, we performed an experiment using one of our RAW264.7-SR-negative clones (4/2 C6) in the presence of chlorpromazine hydrochloride, an inhibitor of clathrin-mediated endocytosis. This experiment demonstrated a similar degree of inhibition of the uptake of 30-nm gold colloids as observed in the chlorpromazine-alone experiment (compare Figures 3C & 3D). However, inhibition of the uptake of the 150-nm gold colloids was significantly decreased in the

presence of both SR and clathrin inhibition (Figure 3D) compared with chlorpromazine only (Figure 3C).

Caveolin-mediated pinocytosis is involved in the uptake of both 30- & 150-nm gold colloids

Since inhibition of SR-mediated phagocytosis and clathrin-mediated pinocytosis did not result in complete inhibition of the uptake of gold colloids, we hypothesized that other pathways must be involved. Caveolin-mediated uptake is another actin-independent form of pinocytosis. We studied whether caveolin is involved in the uptake of gold colloids using filipin III, which inhibits caveolae formation. In the presence of filipin III, a decrease in the uptake of both 30- and 150-nm gold colloids was observed. The uptake of the smaller colloids was slightly more affected than that of the larger particles; however, in both cases a degree of the decrease was not significant compared with negative control (Figure 4a).

When filipin III was added to the RAW264.7-SR-negative cells (clone 4/2 C6), we observed a decrease in the uptake of both the 30- and 150-nm colloids. However, the uptake was not completely blocked and only the inhibition of the 30-nm gold uptake was statistically significant (Figure 4B).

Discussion

We have reported previously that nanoparticle hydrodynamic size can be altered when the nanoparticle is exposed to the biological matrix [19,20], as plasma proteins and other molecules may adhere to the particle and increase its effective hydrodynamic diameter. Hence, this study, which explored the dependence of routes of nanoparticle uptake on particle size, included size measurement before and after incubation in plasma. One of the aims of the current study was to verify whether the ‘rule of thumb’ that particulates smaller than 100 nm cannot be phagocytosed [16], holds for gold colloids. We considered gold colloids with various sizes (5, 10, 30, 50, 80 and 150 nm); however, the light scattering properties of small (less than 30 nm) gold nanoparticles limits their detection (Supplementary Figure 1). Binding of serum proteins (opsonization) causes an increase in particle hydrodynamic size, and after opsonization, the effective hydrodynamic sizes of colloids with nominal sizes of 50 and 80 nm were above the 100-nm limit (data not shown). However, the final hydrodynamic size of the nominally 30-nm particles was below the 100-nm limit after opsonization (Table 1), so our further experiments focused on two test cases: 30 nm, with size below 100 nm both before and after opsonization, and 150 nm, with size above 100 nm both before and after opsonization. Since immune cells recognize and quickly eliminate large aggregates, we verified that the particles used in this study did not aggregate after introduction to cell culture medium. Gold colloids aggregate in PBS or cell culture medium not supplemented with serum; opsonization prevents these particles from aggregation (data not shown, see also [20]). The zeta potential is the electrical potential at the surface separating the molecules that tumble with the nanoparticle in solution and the molecules of the bulk solvent [25]. A nanoparticle’s zeta potential is related to its surface charge, which has been shown to play a role in nanoparticle uptake and plasma–protein binding [26–28]. Measurement of zeta potential allowed us to confirm that in spite of the ‘protein corona’ formed on the particle surfaces (indicated by the increase in particle surface charge), both colloids remain anionic (Table 1). Since endotoxin contamination may confound the results of *in vitro* studies such as cytokine secretion tests [21], and influence phagocytosis by activating macrophages, we have also assessed commercial stocks of 30- and 150-nm gold colloids for endotoxin contamination. Endotoxin was undetectable in both formulations by kinetic turbidity LAL test (<0.005 EU/ml) (Table 1).

There are a variety of different metrics to measure the amount of gold administered to cells and gold uptake: mass of gold; particle number; and surface area. Since each of these methods has advantages and disadvantages and there is no standardized, formally accepted dose metric for nanomaterials, we have tested a variety of dose metrics. The main selection criterion was that the particles be detectable both before and after inhibitors were applied, so that we could be confident in determining the action of the inhibitors. As a result of testing multiple metrics, we selected mass of gold determined by inductively coupled plasma mass spectrometry to dose the cells. We have used RAW264.7 murine macrophage cells as model phagocytes. This model was selected for several reasons:

- This model is well established and well characterized, and has been used in many phagocytosis studies (some of which are reviewed here [14]);
- In contrast to all human monocyte/macrophage cell lines available through the American Type Culture Collection, these cells are adherent, and the method we used to assess particle uptake is limited to adherent cells;
- Use of this cell line allows us to avoid the high variability common in human donors;
- Delivery of siRNA to primary human macrophages or dendritic cells is challenged by the low efficiency of traditional delivery vehicles and safety concerns associated with using higher efficiency retroviral delivery systems.

To summarize the points described above, the discussion in the following section is obtained using the following system: macrophage cell line RAW264.7 (hereafter referred to as macrophages) and its derivative, obtained by viral transduction to deliver siRNA against SR as model professional phagocytes; gold colloids with nominal size of 30 and 150 nm as model gold nanoparticles.

Pretreatment of macrophages with cytochalasin D resulted in decreased uptake of both 30- and 150-nm gold colloids (Figure 1a). We observed a similar decrease in uptake for nanoparticles of both sizes with a lower dose of the inhibitor. Increasing the concentration of cytochalasin D exhibited a complex effect on uptake: the internalization of the large-size colloids (150 nm) was affected to a greater degree (>50%) than that of smaller (30 nm) colloids. This finding suggested that either phagocytosis or macropinocytosis or both, are involved in the uptake of gold colloids. Treatment with 5-(*N*,*N*-dimethyl)amiloride hydrochloride did not result in a significant decrease in the uptake of either 30- or 150-nm gold colloids (Figure 1B). These data do not rule out macropinocytosis as being involved in the uptake of the gold colloids, especially since a macropinocytosis-specific positive control (a viral particle) could not be estimated by our light microscopy method to verify the potency of the inhibitor. However, these data suggest that macropinocytosis does not play a major role in the macrophage uptake of gold colloids, irrespective of their size.

Proinflammatory reactions are commonly reported when phagocytosis of foreign material occurs through complement receptor and FcγR [14]. This is in contrast to phagocytosis mediated by SR, which requires actin polymerization but is not accompanied by a proinflammatory response [14]. Since no cytokine induction (Table 3) and no significant complement activation (Figure 2) were observed, we further focused on the SR-mediated pathway. A decrease in the uptake of 30- and 150-nm gold colloids was observed in both parental RAW264.7 cells pretreated with neutralizing antibody (Figure 3a) and in RAW264.7-SR-negative cells (Figure 3B). The inhibition was more prominent with the smaller (30 nm) nanoparticles than with the larger (150 nm) nanoparticles (Figure 3a). A slight decrease in the uptake of 150-nm gold colloids was observed in cells pretreated with isotype control antibody. The uptake of 30-nm colloids was not affected by the isotype control antibody. The reason for this discrepancy is unknown. However, when isotype

control data for 150-nm gold colloids are compared with data observed with neutralizing antibody, a statistically significant decrease in the presence of high concentration of the neutralizing antibody is seen. These data suggest that the observed inhibition is specific. The results with engineered cells, further support specificity. We tested two clones designated 1/2 and 4/2C6; an inhibition of the uptake was observed in both clones, but was more prominent in clone 1/2. These data are in agreement with results showing the expression of the SR-A in these cells: while SR-A expression in clone 4/2C6 is significantly lower than in parent cells, it is not complete, as evidenced by a weak band on western blot (Figure 3e, the second lane compared with the first lane); a band corresponding to SR-A was below the detection limit of the western blot for clone 1/2. Collectively, these data clearly indicate that small (<100-nm diameter) gold nanoparticles can be phagocytosed, and that this phagocytosis is mediated by the SR. Results obtained with the 150-nm colloids are, in general, more variable than those for the 30-nm colloids. We do not know fully the reason for this difference, but it could originate from the image analysis, in which subtraction of the background and manual selection of the high density area could introduce errors. The small (30 nm) and large (150 nm) particles have different light scattering properties and resultantly, different degrees of brightness for the areas inside the cells corresponding to the particles. The images were analyzed by two scientists to minimize subjectivity, but there is still potential for variability due to the different appearance of these areas on digital images. Since neutralization of SR and inhibition of actin polymerization did not completely abrogate the uptake, we hypothesized that gold colloids may use more than one route to enter the macrophage. An intriguing question whether such alternative route(s) is/are *a priori* available to nanoparticles or stimulated only upon blocking the SR-dependent internalization requires additional investigation.

In order to further investigate routes of nanoparticle uptake by macrophages, we evaluated clathrin- and caveolin-mediated pathways. Clathrin-mediated endocytosis starts with the recruitment of cargo (transferrin-, tyrosine kinase- or G-protein coupled receptors) into developing clathrin-coated pits. These are subsequently formed into clathrin-coated vesicles. The inhibition of this route can be performed using chemical agents such as chlorpromazine hydrochloride. Pretreatment of cells with this inhibitor resulted in significant (close to 50%) inhibition of the uptake of small (30 nm) nanoparticles, but nearly negligible effects on the uptake of the large (150 nm) gold colloids (Figure 3C). Since both colloids are identical in composition, surface charge and were manufactured using a common synthesis procedure, these data suggest that the observed differential sensitivity is due to the particles size, and that clathrin-dependent pinocytosis is involved in uptake of the small (30 nm) but not the large (150 nm) gold nanoparticles. This finding is different from that of an earlier study, which reported the uptake of approximately 90-nm cationic but not anionic polylactid nanoparticles via a clathrin-dependent route [29]. However, our finding is in agreement with a study that demonstrated that the uptake of transferrin-coated gold nanoparticles was clathrin-mediated [4].Since significant (~50%) decreases in the uptake were observed in the absence of SR (Figures 3a & 3B) and in the presence of clathrin-mediated endocytosis inhibitor (Figure 3C), we hypothesized that the uptake of 30-nm colloids could be almost completely blocked by coinhibition of both routes if only these two paths are involved in uptake. To test this hypothesis, we performed the experiment using one of our RAW264.7-SR-negative clones (4/2 C6) in the presence of chlorpromazine hydrochloride, an inhibitor of clathrin-mediated endocytosis. This experiment demonstrated a similar degree of inhibition of the uptake of 30-nm gold colloids as observed in the chlorpromazine-alone experiment (compare Figures 3C & 3D). The results for 150-nm gold colloids were quite different, in that the uptake of 150-nm gold colloids was decreased in the presence of both SR and clathrin inhibition (Figure 3D) compared with when only chlorpromazine was used (Figure 3C). These data suggest that the clathrin-mediated pathway is not a key route for uptake of the 150-nm gold colloids, while SR plays an important role. Since inhibition of

SR-mediated phagocytosis and clathrin-mediated pinocytosis did not result in complete inhibition of the uptake of gold colloids, we hypothesized that other pathways must be involved. Caveolin-mediated uptake is another actin-independent form of pinocytosis. We studied whether caveolin is involved in the uptake of gold colloids using filipin III, which inhibits caveolae formation. In the presence of filipin III, the uptake of both 30- and 150-nm gold colloids decreased. However, the uptake of the smaller colloid was slightly more affected than that of the larger particle. When filipin III was added to the RAW264.7-SR-negative cells (clone 4/2 C6), we observed a decrease in the uptake of both the 30- and 150-nm colloids, but it also did not completely block uptake. This could suggest that other routes are still involved, or that blocking certain routes may activate other endocytic routes to compensate for the inhibition.

In summary, the main finding of this work is that small (less than 100 nm) gold colloids can be phagocytosed, and that this phagocytosis is largely mediated by the macrophage SR. Most known SR-A ligands (e.g., dsDNA, bacterial lipopolysaccharide and bacterial lipoteichoic acid) are anionic; however, it is thought that negative charge is not the only criterion for recognition by the SR-A [30]. Particles used in our study are an example of anionic ligands, which can be taken up via SR. Our data are in agreement with other studies showing internalization of 20-, 50- and 200-nm anionic polystyrene nanoparticles via macrophage SR [12,13].

Conclusion

Within the limits of the used *in vitro* model phagocytic cells, the model test nanoparticles and the multifocal microscopy method, we have demonstrated a difference in the endocytic routes of uptake of gold colloids less than 100 nm in size and greater than 100 nm in size. While actin polymerization is required for the uptake of both 30- and 150-nm gold colloids, macropinocytosis does not appear to be a significant route. The small nanoparticles (30 nm) seem to use a broader spectrum of internalization routes (including SR-, clathrin- and caveolin-mediated pathways), while the larger nanoparticles (150 nm) are preferentially taken up via the SR-route (and, at a lower level, the caveolin-mediated route). The lack of secretion of inflammatory cytokines by phagocytic cells in the presence of tested gold colloids supports the primary role of the SR in their uptake by macrophages *in vitro*.

Future perspective

Understanding the mechanisms of nanoparticle uptake by immune cells is important in the field of nanomedicine, in that it aids in creating specific nanoparticle-based drug delivery systems to target specific tissues, organs or cells, and avoid off-target toxicity. Each individual nanoparticle formulation is unique and therefore, routes and mechanisms of uptake may be specific to particular formulations. While it is impossible to design a study that would address uptake questions applicable to all known nanomaterials, studies aimed at understanding the uptake of individual nanoparticle platforms or individual formulations create a knowledge-base. As multiple concepts are being evaluated and mechanisms of the uptake are understood, such a knowledge-base will expand and, at some point, will allow the identification of trends across a variety of nanoparticle platforms. The results presented in this study involved one type of nanoparticle (anionic, citrate-stabilized gold colloids), an *in vitro* testing in a model macrophage cell line. Future studies combining *in vivo* and *ex vivo* experiments, various sizes and surface functionalities of gold colloids, as well as individual gold-based nanomedicines, and focusing on the events that follow particle uptake through different routes will provide a more complete context for our conclusions.

Supplementary Material

Refer to Web version on PubMed Central for supplementary material.

Acknowledgments

We would like to thank Xunta de Galicia (INBIOMED, 2009/63), Ministerio de Educación y Ciencia (Nanobiomed, Consolider-Ingenio-2010) and SUDOEFEDER (IMMUNONET-SOE1/P1/E014). We thank Jennifer Hall for help in manuscript preparation. We thank Jamie Rodriguez, Sarah Skoczen and Matthew Hansen for excellent technical assistance and Jeffrey Clogston for help with dynamic light scattering and inductively coupled plasma mass spectrometry data interpretation.

The study was supported in whole or, in part, by federal funds from the National Cancer Institute, NIH, under contract N01-CO-12400 and HHSN261200800001E. The content of this publication does not necessarily reflect the views or policies of the Department of Health and Human Services, nor does mention of trade names, commercial products, or organizations imply endorsement by the US Government. Angela França performed her studies at NCL and University of Vigo as part of her undergraduate training sponsored by the Leonardo da Vinci Program.

No writing assistance was utilized in the production of this manuscript.

Bibliography

1. Shukla R, Bansal V, Chaudhary M, et al. Biocompatibility of gold nanoparticles and their endocytotic fate inside the cellular compartment: a microscopic overview. Langmuir. 2005; 21(23): 10644–10654. [PubMed: 16262332]
2. Yang PH, Sun X, Chiu JF, Sun H, He QY. Transferrin-mediated gold nanoparticle cellular uptake. Bioconjug. Chem. 2005; 16(3):494–496. [PubMed: 15898713]
3. Nativo P, Prior IA, Brust M. Uptake and intracellular fate of surface-modified gold nanoparticles. ACS Nano. 2008; 2(8):1639–1644. [PubMed: 19206367]
4. Chithrani BD, Ghazani AA, Chan WC. Determining the size and shape dependence of gold nanoparticle uptake into mammalian cells. Nano Lett. 2006; 6(4):662–668. [PubMed: 16608261]
5. Cui Z, Mumper RJ. Coating of cationized protein on engineered nanoparticles results in enhanced immune responses. Int. J. Pharm. 2002; 238(1–2):229–239. [PubMed: 11996826]
6. Cuna M, Alonso-Sandel M, Remunan-Lopez C, et al. Development of phosphorylated glucomannan-coated chitosan nanoparticles as nanocarriers for protein delivery. J. Nanosci. Nanotechnol. 2006; 6(9–10):2887–2895. [PubMed: 17048495]
7. Kim TH, Jin H, Kim HW, Cho MH, Cho CS. Mannosylated chitosan nanoparticle-based cytokine gene therapy suppressed cancer growth in BALB/c mice bearing CT-26 carcinoma cells. Mol. Cancer Ther. 2006; 5(7):1723–1732. [PubMed: 16891458]
8. Vonarbourg A, Passirani C, Saulnier P, et al. Evaluation of pegylated lipid nanocapsules versus complement system activation and macrophage uptake. J. Biomed. Mater. Res. A. 2006; 78(3):620–628. [PubMed: 16779767]
9. Braden BC, Goldbaum FA, Chen BX, et al. X-ray crystal structure of an anti-Buckminsterfullerene antibody fab fragment: biomolecular recognition of C(60). Proc. Natl Acad. Sci. USA. 2000; 97(22):12193–12197. [PubMed: 11035793]
10. Chen BX, Wilson SR, Das M, Coughlin DJ, Erlanger BF. Antigenicity of fullerenes: antibodies specific for fullerenes and their characteristics. Proc. Natl Acad. Sci. USA. 1998; 95(18):10809–10813. [PubMed: 9724786]
11. von Zur Muhlen C, von Elverfeldt D, Bassler N, et al. Superparamagnetic iron oxide binding and uptake as imaged by magnetic resonance is mediated by the integrin receptor Mac-1 (CD11b/CD18): implications on imaging of atherosclerotic plaques. Atherosclerosis. 2007; 193(1):102–111. [PubMed: 16997307]
12. Kanno S, Furuyama A, Hirano S. A murine scavenger receptor MARCO recognizes polystyrene nanoparticles. Toxicol. Sci. 2007; 97(2):398–406. [PubMed: 17361018]

13. Nagayama S, Ogawara K, Minato K, et al. Fetuin mediates hepatic uptake of negatively charged nanoparticles via scavenger receptor. Int. J. Pharm. 2007; 329(1–2):192–198. [PubMed: 17005341]
14. Aderem A, Underhill DM. Mechanisms of phagocytosis in macrophages. Annu. Rev. Immunol. 1999; 17:593–623. [PubMed: 10358769]
15. Muller K, Skepper JN, Posfai M, et al. Effect of ultrasmall superparamagnetic iron oxide nanoparticles (ferumoxtran-10) on human monocyte–macrophages *in vitro*. Biomaterials. 2007; 28(9):1629–1642. [PubMed: 17178155]
16. Xiang SD, Scholzen A, Minigo G, et al. Pathogen recognition and development of particulate vaccines: does size matter? Methods. 2006; 40(1):1–9. [PubMed: 16997708]
17. Farma JM, Puhlmann M, Soriano PA, et al. Direct evidence for rapid and selective induction of tumor neovascular permeability by tumor necrosis factor and a novel derivative, colloidal gold bound tumor necrosis factor. Int. J. Cancer. 2007; 120(11):2474–2480. [PubMed: 17330231]
18. Paciotti GF, Myer L, Weinreich D, et al. Colloidal gold: a novel nanoparticle vector for tumor directed drug delivery. Drug Deliv. 2004; 11(3):169–183. [PubMed: 15204636]
19. Dobrovolskaia MA, Aggarwal P, Hall JB, McNeil SE. Preclinical studies to understand nanoparticle interaction with the immune system and its potential effects on nanoparticle biodistribution. Mol. Pharm. 2008; 5(4):487–495. [PubMed: 18510338]
20. Dobrovolskaia MA, Patri AK, Zheng J, et al. Interaction of colloidal gold nanoparticles with human blood: effects on particle size and analysis of plasma protein binding profiles. Nanomedicine. 2009; 5(2):106–117. [PubMed: 19071065]
21. Vallhov H, Qin J, Johansson SM, et al. The importance of an endotoxin-free environment during the production of nanoparticles used in medical applications. Nano Lett. 2006; 6(8):1682–1686. [PubMed: 16895356]
22. Conner SD, Schmid SL. Regulated portals of entry into the cell. Nature. 2003; 422(6927):37–44. [PubMed: 12621426]
23. Blander JM, Medzhitov R. On regulation of phagosome maturation and antigen presentation. Nat. Immunol. 2006; 7(10):1029–1035. [PubMed: 16985500]
24. Jones CF, Grainger DW. *In vitro* assessments of nanomaterial toxicity. Adv. Drug Deliv. Rev. 2009; 61(6):438–456. [PubMed: 19383522]
25. Brown, SC.; Palazuelos, M.; Sharma, P., et al. Nanoparticle characterization for cancer nanotechnology and other biological applications. In: Grobmyer, SR.; Moudgil, BM., editors. Methods in Molecular Biology, Cancer Nanotechnology. Humana Press; NY, USA: 2010. p. 39-65.
26. Casals E, Pfaller T, Duschl A, Oostingh GJ, Puntes V. Time evolution of the nanoparticle protein corona. ACS Nano. 2010; 4(7):3623–3632. [PubMed: 20553005]
27. Hellstrand E, Lynch I, Andersson A, et al. Complete high-density lipoproteins in nanoparticle corona. FEBS J. 2009; 276(12):3372–3381. [PubMed: 19438706]
28. Lundqvist M, Stigler J, Elia G, et al. Nanoparticle size and surface properties determine the protein corona with possible implications for biological impacts. Proc. Natl Acad. Sci. USA. 2008; 105(38):14265–14270. [PubMed: 18809927]
29. Harush-Frenkel O, Debotton N, Benita S, Altschuler Y. Targeting of nanoparticles to the clathrin-mediated endocytic pathway. Biochem. Biophys. Res. Commun. 2007; 353(1):26–32. [PubMed: 17184736]
30. Areschoug T, Gordon S. Scavenger receptors: role in innate immunity and microbial pathogenesis. Cell. Microbiol. 2009; 11(8):1160–1169. [PubMed: 19388903]

Websites

101. CytImmune Sciences Inc.. http://cytimmune.com
102. Nanospectra Biosciences. http://nanospectra.com

Box 1

Eight pairwise complimentary oligonucleotides designed based on the cDNA sequences of *mMsr1* and *mMsr2* genes

mMsr1 (mouse Msr1) oligos

- 5′TGCTGTTGACAGTGAGCGCGCAGTTAAATTCCTTGATTTCTAGTGAAGC CACAGATGTAGAAATCAAGGAATTTAACTGCATGCCTACTGCCTCGGA3′
- 5′TGCTGTTGACAGTGAGCGCGTCCAGTCTGTGAAAGAAGAATAGTGAAG CCACAGATGTATTCTTCTTTCACAGACTGGACTTGCCTACTGCCTCGGA3′
- 5′TGCTGTTGACAGTGAGCGATCAGAGTCCGTGAATCTACAGTAGTGAAG CCACAGATGTACTGTAGATTCACGGACTCTGACTGCCTACTGCCTCGGA3′
- 5′TGCTGTTGACAGTGAGCGCTGACACTGCTTGATGTTCAACTAGTGAAGC CACAGATGTAGTTGAACATCAAGCAGTGTCATTGCCTACTGCCTCGGA3′

mMsr2 (mouse Msr2) oligos

- 5′TGCTGTTGACAGTGAGCGATCGCAGTGTCTCAAAGCAGAGTAGTGAAG CCACAGATGTACTCTGCTTTGAGACACTGCGAGTGCCTACTGCCTCGGA3′
- 5′TGCTGTTGACAGTGAGCGCGCTCTGCCTGTGCTCATTCAGTAGTGAAGC CACAGATGTACTGAATGAGCACAGGCAGAGCTTGCCTACTGCCTCGGA3′
- 5′TGCTGTTGACAGTGAGCGAAGTGACCCTGTCCTGCAACACTAGTGAAG CCACAGATGTAGTGTTGCAGGACAGGGTCACTGTGCCTACTGCCTCGGA3′
- 5′TGCTGTTGACAGTGAGCGCAGAGAGCATCTCCTCCGGTTCTAGTGAAGC CACAGATGTAGAACCGGAGGAGATGCTCTCTTTGCCTACTGCCTCGGA3′

Executive summary

- In traditional immunology, phagocytosis is quantified by the number of bacterial cells, yeast or polystyrene beads inside an individual phagocytic cell and reported as the average number of ingested bacteria (yeast and beads) per cell. This measurement is called the 'phagocytic index'. Such a quantifier cannot be used to study nanoparticle uptake, because all the available techniques are not sensitive enough to provide individual particle counts inside cells. To overcome this obstacle, we have developed a method based on multifocal imaging of at least 100 cells per sample, followed by multifocal image analysis using NIH ImageJ software, which measures high-density areas inside cells. We then expressed phagocytic index as the mean area per cell.

- Some earlier studies have attempted to draw general rules for nanoparticle uptake, suggesting that particles less than 100 nm in diameter enter cells via pinocytosis, while larger particles (above 100 nm) are phagocytosed. This conclusion was based on a metastudy of basic research focusing on the uptake of biological particulate matters (such as viruses, bacteria and model polystyrene beads) and therefore, may not be applicable to all engineered nanomaterials. In the present study, we use commercially available citrate-stabilized colloidal gold nanoparticles of two different sizes – one below 100 nm and the other above 100 nm, as a test case to see if this rule extends to colloidal gold nanoparticles.

- To reflect physiological conditions that nanoparticles used in nanomedicine experience after entering the body, the studies with gold colloids were opsonized with human serum. Formation of protein corona around the particles resulted in change in particle hydrodynamic size and zeta potential. Opsonized particles remained anionic and the size of smaller particles was still below the 100 nm of the threshold under investigation.

- Inhibition of actin polymerization resulted in decrease in the uptake of both 30- and 150-nm gold colloids, suggesting that particles with size less than 100 nm can be phagocytosed.

- Further investigation using neutralizing antibody and engineered cell line demonstrated that macrophage scavenger receptor A is involved in phagocytosis of gold colloids *in vitro.*

- Experiments using chemical inhibitors against individual pinocytosis pathways alone or in combination have demonstrated that clathrin- and caveolin-mediated pinocytosis are also involved, and that particles can change the uptake routes depending on what pathway(s) is/are available at a given time.

- Macrophage uptake and resulting liver and spleen accumulation, is a common challenge for nearly all intravenously administered nanomedicines. Each nanoformulation is unique, and it is impossible to design a study that would be broadly applicable to the entire gold-based nanomedicine field, this is why the results of our study need to be explored further with individual gold-based nanomedicines. Studies exploring which physicochemical properties (such as particle size used in our study) influence routes of uptake, will substantially improve the field of nanomedicine.

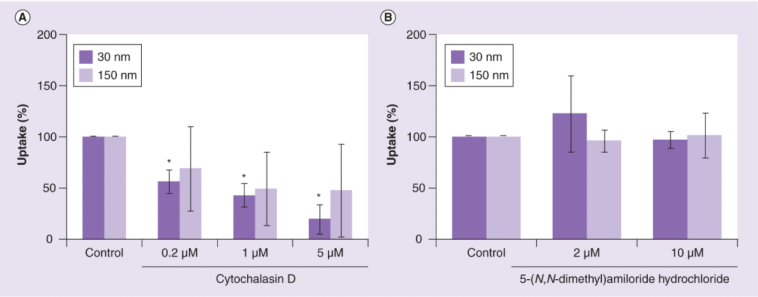

Figure 1. Uptake of gold colloids in the presence of actin polymerization and macropinocytosis inhibitors

RAW264.7 cells were incubated with 30- and 150-nm gold colloids with or without the presence of: **(A)** an inhibitor of actin polymerization (cytochalasin D) or **(B)** an inhibitor of macropinocytosis (5(*N*,*N*,-dimethyl)amiloride hydrochloride). Each sample was analyzed in duplicate and the experiment was repeated twice. Each data point contained at least 100 multifocal images. Shown is mean value (n = 2).

*$p < 0.05$.

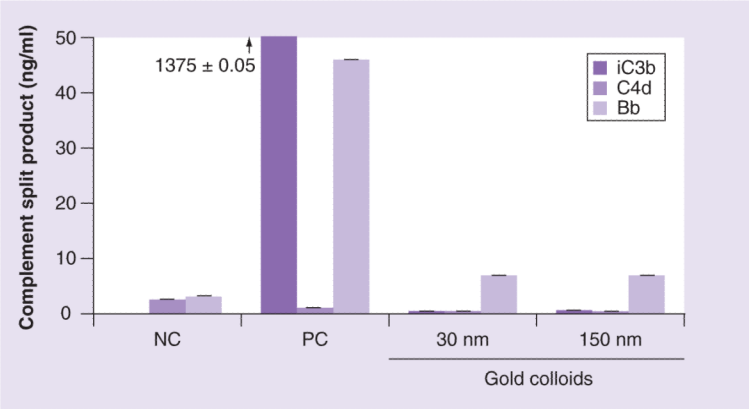

Figure 2. Complement activation

Human sodium–citrate stabilized plasma obtained from three healthy donor volunteers was treated with NC, PC or nanoparticles as described in Materials and methods. Concentration of gold colloids was 50 μg/ml based on total amount of gold determined by the inductively coupled plasma mass spectroscopy. Each sample was analyzed in duplicate. Shown is a mean result (n = 2%CV <10). Cobra venom factor, used as a positive control, activates complement system through an alternative pathway, this is why no activation is seen in the C4d assay. The test results for the positive control in iC3b assay was high (1375.0 ± 0.05 pg/ml). The scale was changed to magnify the lower area; the arrow and the number above the PC value in the iC3b assay are used to show the actual response in this sample.
NC: Negative control; PC: Positive control.

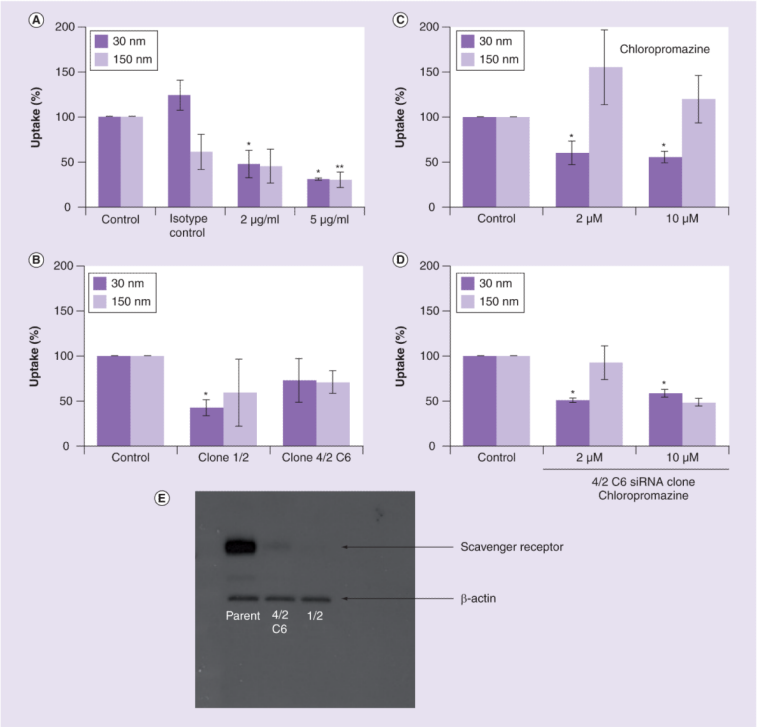

Figure 3. Uptake of gold colloids in the presence of inhibitors of scavenger receptor and clathrin

RAW264.7 cells were incubated with 30- and 150-nm gold colloids with or without the presence of inhibitors that block the scavenger receptor and clathrin-mediated pathway. **(A)** Scavenger receptor was inhibited by MSR-1-specific neutralizing antibodies. **(B)** Expression of scavenger receptor was inhibited by siRNA. **(C)** Clathrin-mediated uptake was inhibited with chloropromazine hydrochloride. **(D)** Inhibition of both clathrin and scavenger receptor-mediated uptake was achieved by incubating nanoparticles with siRNA-bearing cells in the presence of chloropromazine hydrochloride. Each sample was analyzed in duplicate and the experiment was repeated twice. Each data point contained at least 100 multifocal images. Shown is mean value (n = 2). **(E)** Analysis of the SR-A expression by parental RAW264.7 cells and cells transduced with SR-A-specific siRNA bearing construct. Cell lysates were analyzed by western blot using monoclonal antibody directed against SR-A to control SR-A expression and anti-β-actin antibody to control protein loading.

*$p < 0.05$ when compared with negative control; **$p < 0.05$ when compared with isotype control.

SR-A: Scavenger receptor A.

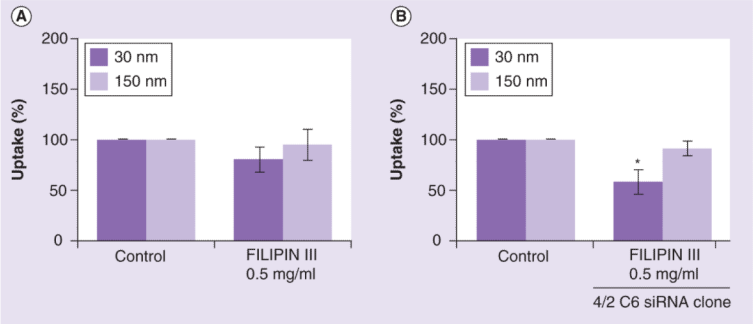

Figure 4. Uptake of gold colloids in the presence of inhibitors of scavenger receptor and caveolin

RAW264.7 cells were incubated with 30- and 150-nm gold colloids with or without the presence of inhibitors that block scavenger receptor and caveolin-mediated pathway. **(A)** Caveolin-mediated uptake was inhibited with filipin III. **(B)** Inhibition of both caveolin- and scavenger receptor-mediated uptake was achieved by incubating nanoparticles with siRNA bearing cells in the presence of filipin III. Each sample was analyzed in duplicate and the experiment was repeated twice. Each data point contained at least 100 multifocal images. Shown is the mean value (n = 2).

*$p < 0.05$.

Table 1

Particle size and zeta potential were analyzed as described in the experimental section.

Particles (nominal size)	Size by DLS Intensity-weighted peak (nm)		Zeta potential (mV)		Gold concentration by ICP-MS (μg/ml)	Endotoxin (EU/ml[†])
	Before	*After*	*Before*	*After*		
30 nm	34.4 ± 0.2	94.8 ± 0.2	−38.2 ± 1.2	−16.4 ± 0.6	48.0 ± 3.9	<0.005
150 nm	149.8 ± 0.7	263.6 ± 4.7	−46.3 ± 0.9	−20.4 ± 1.9	42.5 ± 3.7	<0.005

[†]1 ml of commercial stock contained 48.0 ± 3.9 or 42.5 ± 3.7 μg of gold for 30- and 150-nm gold colloids, respectively.

Shown is mean result plus or minus standard deviation based on 12 data points (n = 12). Before and after refer to opsonization with human serum. For endotoxin quantification each sample was analyzed three times, each analysis was performed in duplicate, shown is mean result (%CV less than 20).

DLS: Dynamic light scattering; ICP-MS: Inductively coupled plasma mass spectrometry.

Table 2

Inhibitors used in the present study.

Endocytic portals	Main proteins implicated	Main inhibitor	Effect induced by inhibitor	Notes
Phagocytosis	Actin, dynamin	Cytochalasin D	Prevents F-actin polymerization	
Macropinocytosis	Actin, dynamin	5-(*N*,*N*-dimethyl)amiloride hydrochloride	Inhibitor of membrane Na^+/H^+ ATPase	Cytochalasin D also affects macropinocytosis
Clathrin mediated	Dynamin; clathrin triskelions also actin and many others	Chlorpromazine hydrochloride	Blocks endocytosis via clathrin-coated pits	
Caveolin mediated	Caveolins, also actin and others	Filipin III	Inhibitis caveolae formation	
Clathrin/caveolin-independent endocytosis	Actin, GRAF1	Combinations of inhibitors		

This is a summary of inhibitors used in our study. Shown are the effects induced by the inhibitor and the mechanism of its action [22–24].

Table 3

Cytokine secretion by peripheral blood mononuclear cells.

pg/ml	Treatment	IFN- γ	IL-1 β	IL-2	IL-4	IL-5	IL-8	IL-10	IL-12p70	IL-13	TNF- α
Donor 1	NC	1.4	0.7	1.3	0.4	0.8	244.8	4.0	0.2	0.6	2.6
	PC	4007.6	8159.0	93.5	5.9	6.8	981.5	484.6	24.9	13.3	>10,000
	AuNP 150 nm	1.1	5.7	0.8	0.5	0.5	120.5	15.0	0.8	1.6	3.4
	AuNP 30 nm	5.3	2.6	1.8	1.4	0.8	53.6	10.4	1.2	1.6	3.5
Donor 2	NC	7.0	1.2	2.0	1.8	1.3	202.3	5.9	2.2	2.6	3.1
	PC	345.4	1956.8	16.4	2.5	1.9	1295.7	323.2	3.0	6.2	1980.6
	AuNP 150 nm	0.9	0.6	0.4	0.6	0.2	41.5	6.5	0.6	0.8	1.6
	AuNP 30 nm	0.2	0.2	0.2	0.2	0.2	39.9	4.9	0.3	0.7	1.8
Donor 3	NC	1.7	2.8	0.7	0.7	0.9	323.3	3.1	0.9	2.4	3.0
	PC	5959.0	7371.8	25.2	7.6	8.9	1182.6	655.2	112.2	13.8	>10,000
	AuNP 150 nm	0.4	0.9	0.2	0.5	0.3	38.0	4.2	0.9	0.8	1.5
	AuNP 30 nm	0.0	0.5	0.1	0.4	0.1	24.9	3.2	0.2	0.3	1.0
	Detection limit	0.9	0.2	0.2	0.2	0.1	0.1	0.3	0.2	0.4	0.2

Human peripheral blood mononuclear cells were isolated from freshly drawn whole blood obtained from healthy donor volunteers and treated with controls or nanoparticles as described in Materials and methods section. Particles were used at final concentration of 42.5 μg/ml based on the amount of total gold determined by the inductively coupled plasma-mass spectrometry. Treatment time: 24 h. Each sample was analyzed in duplicate. Shown is a mean value (%CV >25).

PC: Positive control; NC: Negative control (phosphate-buffered saline).